Journal of Systems Engineering and Electronics
Vol. 31, No. 6, December 2020, pp.1318 – 1329

Airship aerodynamic model estimation using unscented Kalman filter

WASIM Muhammad* and ALI Ahsan

Department of Electrical Engineering, University of Engineering and Technology, Taxila 47080, Pakistan

Abstract: An airship model is made-up of aerostatic, aerodynamic, dynamic, and propulsive forces and torques. Besides others, the computation of aerodynamic forces and torques is difficult. Usually, wind tunnel experimentation and potential flow theory are used for their calculations. However, the limitations of these methods pose difficulties in their accurate calculation. In this work, an online estimation scheme based on unscented Kalman filter (UKF) is proposed for their calculation. The proposed method introduces six auxiliary states for the complete aerodynamic model. UKF uses an extended model and provides an estimate of a complete state vector along with auxiliary states. The proposed method uses the minimum auxiliary state variables for the approximation of the complete aerodynamic model that makes it computationally less intensive. UKF estimation performance is evaluated by developing a nonlinear simulation environment for University of Engineering and Technology, Taxila (UETT) airship. Estimator performance is vali dated by performing the error analysis based on estimation error and 2-σ uncertainty bound. For the same problem, the extended Kalman filter (EKF) is also implemented and its results are compared with UKF. The simulation results show that UKF successfully estimates the forces and torques due to the aerodynamic model with small estimation error and the comparative analysis with EKF shows that UKF improves the estimation re sults and also it is more suitable for the under-consideration problem.

Keywords: airship, unscented Kalman filter (UKF), extend Kalman filter (EKF), state estimation, aerodynamic model estimation.

DOI: 10.23919/JSEE.2020.000102

1. Introduction

The past few decades have seen an emergence of aerial robots for many airborne missions. Due to the enormous applications, it remains a hot topic of technological and scientific research. Although heavier than air, aerial robots have enjoyed widespread utility. However, their limited duration of flight and low payload capacity constraints restrain their use in many applications. For example, agriculture and environmental monitoring require aerial robots to fly with slow speed at low altitudes, and providing a platform for communication relay necessitates the long-duration stay at high altitudes. For these sorts of applications, the airship can be a potential candidate due to some of its unique properties. As it can remain airborne for a long duration with the minimum power consumption because lighter than air nature provides it an aerostatic lift to stay aloft. It requires the minimum maintenance and operational cost [1]. It can fly at high altitudes and a hybrid airship concept can provide heavy cargo lifting capabilities. However, it is required to develop the autonomous guidance and flight controller for the airship to achieve specific application goals.

Lots of efforts have been made for the development of an autonomous airship platform that can be used for different human-planned missions [2,3]. Regardless of notable progress made in this field, much needs to be explored so that the airship can be used as an aerial robot [4] especially in the area of autonomous control. The successful design of an efficient control system necessitates accurate model information. In the literature, many contributions can be found, which were directed to the development of different control models for airship autonomous navigation. In [5,6], linearized equations of motion can be found by using a small perturbation techniques. In [7], a method for identifying linearized longitudinal and lateral models from flight data was suggested for which Lotte airship was used as an experimental platform. The trust-region reflective least square approach in [8] and radial bases function neural networks (RBFNNs) in [9] were utilized for identifying linearized longitudinal and lateral models from flight data of University of Engineering and Technology, Taxila (UETT) airship. Linearized models were utilized for flight controller design in [10]. As these models are linearized in equilibrium flight conditions so their performance can be assured only around the equilibrium points.

Manuscript received November 20, 2019.
*Corresponding author.

In [11], a reduced nonlinear control model was used for positioning control of airships. The reduced nonlinear models are obtained by making the modelling assumption that effects of roll rate, pitch rate, and vertical velocity on airship planar motion are negligible. In [12,13], an attitude controller and a yaw controller were designed based on reduced attitude and yaw control models respectively. Performance of the controller using reduced nonlinear control models degrades under abrupt disturbances and if the made assumptions are violated. An airship full nonlinear 6-DOF model was used for controller design in [14,15]. Although considering the complete model for controller design increases the controller performance it necessitates the model accuracy. In the case of an airship, its complete 6-DOF nonlinear model is made up of dynamic, aerostatic, aerodynamic, and propulsion forces and torques. Besides others, the calculation of aerodynamic forces has remained an issue [16]. In the literature, these are calculated by using famous wind tunnel experiments and potential flow theory.

Wind tunnel experiments are conducted in large tubes where scaled physical models of aerial vehicles are mounted at a particular location in the tunnel. The tunnel tries to mimic the actual environment that an air vehicle may experience while moving through the air. Air is blown on the model with different angles. In the model, force and pressure measuring sensors are placed at different locations. Data for forces and torques acting on an aerial vehicle due to the incident air are collected for various sideslips, and angle of attacks. Later, from this data, drag, side, and lift force coefficients and rolling, pitching and yaw torques coefficients are estimated. These experiments played an important role in the dynamic analysis of airships in those days when comprehensive aerodynamic models for airships were not available. Lots of these experiments were performed between 1910 to 1976. In [17, 18], data of wind tunnel tests performed between 1910 to 1920 for different British airships could be found. In [18], the data of wind tunnel tests that were performed for airships up to 1976 were covered. Other than that, many reports of the advisory committee for aeronautics established by the USA and the Great Britain, cover the wind tunnel experiments. These experiments are still important for the dynamic analysis of modern airships like [19] covers the data for YEZ-2A airship, Lotte [20] and the TCOM-250 aerostats [21] . However, it is difficult to conduct these experiments because they are expensive. Hence in the literature, apart from wind tunnel experiments, aerodynamic models based on the potential flow theory are also proposed.

The initial work on the aerodynamic model using the potential flow theory can be found in the report published by Munk in 1924 [22]. In [23], Munk's work was improved by adding the crossflow drag effects. In [21, 24], hull and fin interactions were considered in aerodynamic model equations. Based on the work of [21], Muller in [25], proposed the comprehensive aerodynamic model that could calculate the 3-DOF forces and 3-DOF torques affecting the airship motion due to aerodynamic phenomena. However, the model was deficient because of ignoring the damping effects due to airship pitch, roll, and yaw motions. In [26], Muller's work was improved by suggesting the aerodynamic model equations that incorporate the damping terms. The aerodynamic models suggested in [25,26] depend on airship geometrical parameters, for example, airship length, surface area, and volume, and also on few coefficients that depend on wind tunnel data. Further, they made an assumption that the airship shape does not change during the course of a flight. However, the airship envelope may experience unforeseen shape changes due to its flexible nature. Therefore, the actual aerodynamic forces may differ from the forces calculated by these models.

To avoid the errors of analytical calculation methods and conducting expensive wind tunnel experiments, in this paper an efficient and cost-effective method for estimating forces and torques due to aerodynamics is proposed by using the uncented Kalman filter (UKF). Although this problem can be solved by using fuzzy logic, nonlinear observers, neural networks, or adaptive control methods as given in [14,15,27,28], UKF provides an additional advantage of estimating actual aerodynamic forces and aerodynamic torques rather than complying with them.

UKF is a nonlinear version of the Kalman filter and it has been utilized in many potential applications. Based on the covariance of the current state estimate, the UKF estimation method chooses several sample points around the current state estimate. Then these sample points are propagated through the nonlinear function to get a more accurate estimate of mean and covariance. Unlike the extended Kalman filter (EKF), UKF avoids the computation of the state Jacobian matrix. Airship state and parameter estimation using UKF was reported in [29−31]. In [29], UKF was designed for airship states and aerodynamic model parameters estimation. In [30,31], airship attitudes and linear velocities were estimated by using UKF.

To apply the Kalman filter algorithm, it is necessary to represent the system in state-space form. The unknown parameters of interest like disturbances, system parameters, unknown forces, or torques are accommodated as an additional state variable. As the number of states increases, filter computational complexity also increases. In [29], UKF was designed for the estimation of aerodynamic model parameters. However, the given method is computationally intensive because it introduces more than 50 augmentative state variables. In the proposed work, for reducing computational complexity, instead of estimating aerodynamic model parameters, a complete aerodynamic model is estimated by introducing only six new state variables.

In the proposed estimation method, UKF estimates the airship complete states vector along with aerodynamic forces and torques. It assumes that the airship position and attitude's estimates are available. As of now off-the-shelf solutions for estimating aerial vehicle attitude and position are available [32, 33], this assumption is not restrictive. The method also assumes that the aerodynamic model is not known. As airships possesses slow dynamics compared to conventional aerial vehicles, further assumption is made that the aerodynamic forces and torques' rate of change is zero. The proposed contribution provides the online estimation scheme for an aerodynamic model that can be utilized for the development of nonlinear autonomous flight controllers for an airship. It can be a cost-effective alternative to expensive wind tunnel experiments, and it avoids the error of analytical calculation methods. For the validation of the proposed method, a nonlinear simulation environment for "UETT" airship is developed based on the algorithm given in [26]. The airship is provided with propeller input, rudder, and elevator deflections.

The rest of the paper is organized as follows: Section 2 explains the airship 6-DOF nonlinear model. In Section 3, a modified nonlinear model is presented for estimator design, the airship model is also represented in a nonlinear state-space suitable for the implementation of the UKF algorithm and the UKF algorithm is given at the end of this section. Section 4 covers the simulation results and in Section 5 concluding remarks and future work are given.

2. Airship 6-DOF nonlinear model

An airship has few components: envelope, gondola, airbags, thrusters, aerodynamic control surfaces rudders, and elevators. Gondola exists beneath the envelop and thrusters are attached to both sides as shown in Fig. 1. In "UETT" airship case, variable thrusting is not available and because of a single motor for propellers tilting, limited vector thrusting is available. Rudders and elevators are mounted in plus configuration at the tail of the airship. The envelope is filled with low-density Helium gas. Airbags exist inside the envelope to control its buoyancy. Two reference frames are used for assessing its navigation. A body reference frame $o_b x_b y_b z_b$ is attached to the center of volume (CV) of an airship. The second is an inertial frame $O_i X_i Y_i Z_i$, which is located at any reference point on earth as shown in Fig. 1.

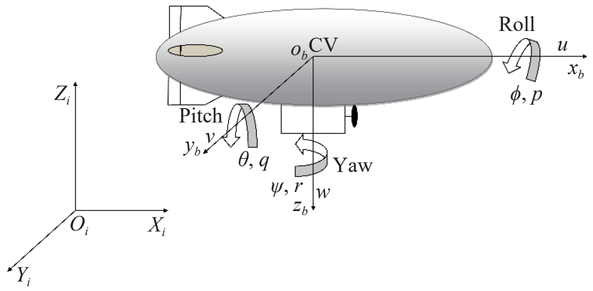

Fig. 1 Coordinate system of an airship

Propulsion and aerodynamic control forces act on an airship in the body frame and produce body axes accelerations. Then the transformation matrix is utilized to transform them into the inertial frame, for assessing airship navigation with respect to the inertial frame. Let $\boldsymbol{\zeta} = [x, y, z]^{\mathrm{T}}$ be the airship position with respect to the inertial frame and its attitude are represented by $\boldsymbol{\varsigma} = [\phi, \theta, \psi]^{\mathrm{T}}$ where ϕ is the roll angle, θ is the pitch angle and ψ is the yaw angle. $\boldsymbol{v} = [u, v, w]^{\mathrm{T}}$ is a vector of linear velocities with respect to the airship body frame where u is the forward velocity, v is the sway velocity and w is the vertical velocity. $\boldsymbol{\omega} = [p, q, r]^{\mathrm{T}}$ is a vector of angular velocities with respect to the body frame, where p represents the roll rate, q is the pitch rate and r is the yaw rate. $\boldsymbol{\xi} = [\boldsymbol{\zeta}^{\mathrm{T}}, \boldsymbol{\varsigma}^{\mathrm{T}}]^{\mathrm{T}}$, $\boldsymbol{\upsilon} = [\boldsymbol{v}^{\mathrm{T}}, \boldsymbol{\omega}^{\mathrm{T}}]^{\mathrm{T}}$ are the compact representation of inertial frame and body frame linear and angular motion variables.

The equations of motion for the airship are the modified form of equations for an underwater vehicle, whose basic formulation can be found in [27]. The vector form of the airship model can be represented by

$$\dot{\boldsymbol{\upsilon}} = \boldsymbol{M}^{-1}(\boldsymbol{F}_d + \boldsymbol{F}_{Ad} + \boldsymbol{F}_{As} + \boldsymbol{F}_P) \tag{1}$$

where $\dot{\boldsymbol{\upsilon}} \in \mathbf{R}^{6\times 1}$ is the vector containing body axes linear and angular accelerations. $\boldsymbol{M} \in \mathbf{R}^{6\times 6}$ is a mass matrix, $\boldsymbol{F}_d \in \mathbf{R}^{6\times 1}$ is a dynamic force vector which is composed of centripetal and Coriolis forces and moments, $\boldsymbol{F}_{Ad} \in \mathbf{R}^{6\times 1}$ is an aerodynamic force vector, $\boldsymbol{F}_{As} \in \mathbf{R}^{6\times 1}$ is an aerostatic force vector which is composed of gravity and buoyancy forces, and $\boldsymbol{F}_p \in \mathbf{R}^{6\times 1}$ is the propulsion force vector which is composed of forces and torques acting on the airship due to propellers. Here, $\mathbf{R}$ represents the set of real numbers.

The airship mass matrix is given in

$$\boldsymbol{M} = \begin{bmatrix} m_x & 0 & 0 & 0 & m_6 & 0 \\ 0 & m_y & 0 & m_5 & 0 & m_8 \\ 0 & 0 & m_z & 0 & m_7 & 0 \\ 0 & m_1 & 0 & J_x & 0 & -J_{xz} \\ m_2 & 0 & m_3 & 0 & J_y & 0 \\ 0 & m_4 & 0 & -J_{xz} & 0 & J_z \end{bmatrix}. \tag{2}$$

The elements of the mass matrix are defined [34] as

$$\begin{cases} m_x = m - X_{\dot{u}} \\ m_y = m - Y_{\dot{v}} \\ m_z = m - z_{\dot{w}} \\ m_6 = ma_z - X_{\dot{q}} \\ m_5 = -ma_z - Y_{\dot{p}} \\ m_8 = ma_x - Y_{\dot{r}} \\ m_7 = -ma_x - z_{\dot{q}} \\ m_1 = -ma_z - L_{\dot{v}} \\ m_2 = ma_z - M_{\dot{u}} \\ m_3 = -ma_x - M_{\dot{w}} \\ m_4 = ma_x - N_{\dot{v}} \end{cases}$$

where $X_{\dot{u}}$, $Y_{\dot{v}}$, $Z_{\dot{w}}$, $X_{\dot{q}}$, $Y_{\dot{p}}$, $Y_{\dot{r}}$ and $Z_{\dot{q}}$ are the virtual mass terms, $L_{\dot{v}}$, $M_{\dot{u}}$, $M_{\dot{w}}$ and $N_{\dot{v}}$ are the virtual inertia terms, (a_x, a_z) is the location of the center of gravity (CG) with respect to the CV, and m is the total mass of the airship. The airship mass matrix contains the added mass terms. As the mass of displaced air is approximately equal to the actual airship mass so in airship cases added mass effects cannot be ignored and they are incorporated in the airship mass matrix as a virtual mass and inertia terms.

Using the defined position, attitude, and velocities variables, the vector form of the airship kinematic model will be

$$\dot{\boldsymbol{\xi}} = \boldsymbol{R}(\boldsymbol{\varsigma})\boldsymbol{\upsilon} \tag{3}$$

where

$$\boldsymbol{R}(\boldsymbol{\varsigma}) = \begin{bmatrix} \boldsymbol{R}_1(\boldsymbol{\varsigma}) & \boldsymbol{0}_{3\times3} \\ \boldsymbol{0}_{3\times3} & \boldsymbol{R}_2(\boldsymbol{\varsigma}) \end{bmatrix}. \tag{4}$$

$\boldsymbol{0}_{3\times3} \in \mathbf{R}^{3\times3}$ is a zero matrix that has all elements with zero value. $\boldsymbol{R}_1(\boldsymbol{\varsigma})$ represents the rotation matrix that transforms the body axes linear velocities to the inertial reference frame position derivative and $\boldsymbol{R}_2(\boldsymbol{\varsigma})$ transforms the body axes angular velocities to the inertial frame attitude rates. The expressions of $\boldsymbol{R}_1(\boldsymbol{\varsigma})$ and $\boldsymbol{R}_2(\boldsymbol{\varsigma})$ matrices are given in (5) and (6) with a simplification of sin(·), tan(·), sec(·), and cos(·) as $s_{(\cdot)}$, $t_{(\cdot)}$, $se_{(\cdot)}$ and $c_{(\cdot)}$ respectively.

$$\boldsymbol{R}_1(\boldsymbol{\varsigma}) = \begin{bmatrix} c_\psi c_\theta & c_\psi s_\theta s_\phi - s_\psi c_\phi & c_\psi s_\theta c_\phi + s_\psi s_\phi \\ s_\psi c_\theta & s_\theta s_\phi s_\psi + c_\psi c_\phi & s_\psi c_\phi s_\theta - c_\psi s_\phi \\ -s_\theta & c_\theta s_\psi & c_\theta c_\psi \end{bmatrix} \tag{5}$$

$$\boldsymbol{R}_2(\boldsymbol{\varsigma}) = \begin{bmatrix} 1 & s_\phi t_\theta & c_\phi t_\theta \\ 0 & c_\phi & -s_\phi \\ 0 & s_\phi se_\theta & c_\phi se_\theta \end{bmatrix} \tag{6}$$

The airship nonlinear model can be compactly represented by assuming that the body axes forces and torques acting on the airship are given by $\boldsymbol{f} = \boldsymbol{F}_d + \boldsymbol{F}_{Ad} + \boldsymbol{F}_{As} + \boldsymbol{F}_P$, where

$$\boldsymbol{f} = [\ f_u \quad f_v \quad f_w \quad \tau_l \quad \tau_m \quad \tau_n\ ]^{\mathrm{T}}. \tag{7}$$

Then the airship model representation in the form of nonlinear state-space compatible for estimator design can be represented by the following equation:

$$\begin{bmatrix} \dot{\boldsymbol{\xi}} \\ \dot{\boldsymbol{\upsilon}} \end{bmatrix} = \begin{bmatrix} \boldsymbol{R}(\boldsymbol{\varsigma}) & \boldsymbol{0}_{6\times6} \\ \boldsymbol{0}_{6\times6} & \boldsymbol{M}^{-1} \end{bmatrix} \begin{bmatrix} \boldsymbol{\upsilon} \\ \boldsymbol{f} \end{bmatrix} \tag{8}$$

where the elements of body axes force and torques vector $\boldsymbol{f}$ will be

$$\begin{aligned} f_u = {} & -m_z wq + m_y rv + m\left[a_x\left(q^2+r^2\right) - a_z rp\right] + \\ & \frac{1}{2}\rho V_0^2 S\left[C_{X1}\cos^2\alpha\cos^2\beta C_{X2}\left(\sin(2\alpha)\sin\frac{\alpha}{2} + \right.\right. \\ & \left.\left.\sin\,(2\beta)\sin\frac{\beta}{2}\right) + C_{X3}\right] - (W-B)\sin\theta + \\ & (T_{ds}+T_{dp})\cos\mu, \end{aligned} \tag{9}$$

$$\begin{aligned} f_v = {} & -m_x ur + m_z pw + m[-a_x pq - a_z rq] + \\ & \frac{1}{2}\rho V_0^2 S\left[C_{Y1}\sin(2\beta)\cos\frac{\beta}{2} + C_{Y2}\sin(2\beta) + \right. \\ & \left. C_{Y3}\sin|\beta|\sin\beta + C_{Y4}(\delta_{RT}+\delta_{RB})\right] + \\ & (W-B)\cos\theta\sin\phi, \end{aligned} \tag{10}$$

$$\begin{aligned} f_w = {} & -m_y vp + m_x qu + m\left[-a_x rp + a_z\left(q^2+p^2\right)\right] + \\ & \frac{1}{2}\rho V_0^2 S\left[C_{z1}\cos\frac{\alpha}{2}\sin(2\alpha) + C_{z2}\sin(2\alpha) + \right. \\ & \left. C_{z3}\sin\alpha\sin|\alpha| + C_{z4}(\delta_{EL}+\delta_{ER})\right] + \\ & (W-B)\cos\theta\cos\phi - (T_{ds}+T_{dp})\sin\mu, \end{aligned} \tag{11}$$

$$\begin{aligned} \tau_l = {} & -(J_z - J_y)rq + J_{xz}pq + ma_z(ur - pw) + \\ & \frac{1}{2}\rho V_0^2 LS\left[C_{L1}(\delta_{EL}-\delta_{ER}+\delta_{RB}-\delta_{RT}) + C_{L2}\sin\beta\sin|\beta| + \right. \\ & \left.\frac{1}{2}\rho S\,(C_{L3}r|r| + C_{L4}p|p|)\right] + a_z W\cos\theta\sin\phi + \\ & (T_{dp}-T_{ds})\sin\mu d_y + (T_{ds}+T_{dp})(d_z\cos\mu - d_x\sin\mu), \end{aligned} \tag{12}$$

$$\begin{aligned} \tau_m = {} & -(J_x - J_z)pr + J_{xz}\left(r^2 - p^2\right) + m[a_x(vp - qu) - \\ & a_z(wq - rv)] + \frac{1}{2}\rho V_0^2 LS\left[C_{M1}\sin(2\alpha)\cos\frac{\alpha}{2} + \right. \\ & C_{M2}\sin(2\alpha) + C_{M3}\sin|\alpha|\sin\alpha + C_{M4}(\delta_{EL}+\delta_{ER}) + \\ & \left.\frac{1}{2}\rho S\,(C_{M5}q|q|)\right] - (a_z W - b_z B)\sin\theta - \\ & (a_x W - b_x B)\cos\theta\cos\phi, \end{aligned} \tag{13}$$

$$\begin{aligned} \tau_n = {} & -(J_y - J_x)qp - J_{xz}qr + m[-a_x(ur - pw)] + \\ & \frac{1}{2}\rho V_0^2 LS\left[C_{N1}\sin(2\beta)\cos\frac{\beta}{2} + C_{N2}\sin(2\beta) + \right. \\ & \left. C_{N3}\sin|\beta|\sin\beta + C_{N4}(\delta_{RT}+\delta_{RB}) + \frac{1}{2}\rho S\,(C_{N5}r|r|)\right] + \\ & a_x W\cos\theta\sin\phi + (T_{dp}-T_{ds})\cos\mu d_y, \end{aligned} \tag{14}$$

where α represents the angle of attack, β represents the side slip angle, V_0 represents the velocity of airship, ρ represents the air density, S represents the airship total surface area, W represents the weight of airship, B represents the buoyancy force, L represents the airship length, d represents the airship diameter,

$$\bar{m}=\frac{B}{g},$$

$$\bar{I}_y=\frac{\bar{m}(L^2+d^2)}{20}.$$

Drag force coefficients:

$$C_{X1}=-[C_{Dh0}S_h+C_{Df0}S_f+C_{Dg0}S_g],$$
$$C_{X2}=(K_2-K_1)\eta_K I_1 S_h.$$

Side force coefficients:

$$C_{Y1}=C_{X2},$$
$$C_{Y2}=-\frac{1}{2}\left(\frac{\partial C_L}{\partial \alpha}\right)_f S_f\eta_f,$$
$$C_{Y3}=-[C_{Dch}J_1S_h+C_{Dcf}S_f+C_{Dcg}S_g],$$
$$C_{Y4}=-\frac{1}{2}\left(\frac{\partial C_L}{\partial \delta}\right)_f S_f\eta_f.$$

Lift force coefficients:

$$C_{z1}=C_{y1}C_{z2}=C_{y2}C_{z3}=-[C_{Dch}J_1S_h+C_{Dcf}S_f].$$

Rolling torque coefficients:

$$C_{L1}=\left(\frac{\partial C_L}{\partial \delta}\right)_f S_f\eta_f l_{f3},$$
$$C_{L2}=-C_{Dcg}S_g l_{gz}.$$

Pitching torque coefficients:

$$C_{M1}=-(K_1-K_2)\eta_K I_3 S_h L C_{M2}=-\frac{1}{2}\left(\frac{\partial C_L}{\partial \alpha}\right)_f S_f\eta_f l_{f1},$$
$$C_{M3}=-[C_{Dch}J_2S_hL+C_{Dcf}S_f l_{f2}],$$
$$C_{M4}=-\frac{1}{2}\left(\frac{\partial C_L}{\partial \delta}\right)_f S_f\eta_f l_{f1}.$$

Yawing torque coefficients:

$$C_{Nj}=-C_{Mj},$$

where

$$I_1=\pi\frac{b^2}{V^{2/3}}\left(1-f^2\right),$$

$$I_3=\pi\frac{b^2}{3LV^{2/3}}\left(a_1-2a_2f^3-3a_1f^2\right)-\frac{x_{cv}}{L}I_1,$$

$$J_1=\frac{b}{2V^{2/3}}\left(a_1\frac{\pi}{2}+a_2\sqrt{1-f^2}f+2a_2\sin^{-1}(f)\right),$$

$$J_2=J_1\frac{a_1-x_{cv}}{L}+\frac{2b}{3LV^{2/3}}(a_2^2-a_1^2-a_2^2\left(1-f^2\right)^{3/2},$$

$$f=\frac{l_h-a_1}{a_2},$$

$$x_{cv}=a_1+\frac{3}{8}(a_2-a_1).$$

K_1, K_2, $K^{'}$ are the Lamb's inertia ratio. C_{Dh0}, C_{Df0}, C_{Dg0} are the zero-incidents, C_{Dch}, C_{Dcf}, C_{Dcg} are the crossflow drag coefficients of hull, fins and gondola respectively. $\left(\frac{\partial C_L}{\partial \alpha}\right)_f$ is a derivative of fin lift-coefficient with respect to the angle-of-attack at zero incidence. $\left(\frac{\partial C_L}{\partial \delta}\right)_f$ is a derivative of fin lift-coefficient with respect to the flap deflection angle. S_h, S_f and S_g are the hull, fin and gondola reference areas. l_{f1}, l_{f2}, l_{f3}, l_{gx}, l_{gz} and l_h are the geometrical parameters of hull. η_f is the fin efficiency factor. η_k is the hull efficiency factor.

The origin of the body frame is located at the airship's CV. For the double-ellipsoid geometry, the CV is located on the x-axis at the point x_{cv}.

3. UKF design for airship aerodynamic forces and torques estimation

UKF is a nonlinear estimator and it has been utilized for many applications. The UKF algorithm does the so-called unscented transformation to capture the propagation of the statistical properties of state estimates through the system nonlinear function. The algorithm first generates a set of state values called sigma points. These sigma points capture the mean and covariance of the state estimates. It uses each of the sigma points as an input to the state transition and measurement functions to get a new set of transformed state points. The mean and covariance of the transformed points are then used to obtain state estimates and state estimation error covariance.

Apart from the estimation of system states, the Kalman filter algorithm and its variants are also used for estimating the external disturbances, unknown system parameters, and system faults. The system is represented in the state-space form before applying the Kalman filter algorithm or its variants. Additional state variables are incorporated in the actual system model for estimating system faults, external disturbances, or system parameters. And the Kalman filter algorithm is applied to the new extended system representation. In such a way, it estimates the original system states as well as the augmentative states. However, it requires the modeling information of the augmentative states. Therefore, it is better if the equations for the augmentative states are available, but if not, two choices can be made as given in [35]. First, if the rate of change of new state variables is very slow then they can be assumed zero. Second, if they vary with a constant amount, then their rates of change can be assumed constant. Since external disturbances to the system is a low-frequency phenomenon, it is usually modeled with augmentative states having zero rates of change. This method was utilized in [36] for estimating disturbances on the twin rotor aerodynamic system (TRAS) using EKF. In their work, they used two additional state variables, one for estimating disturbances acting on TRAS longitudinal dynamics and the other one on its lateral dynamics. In [29], the author utilized UKF and EKF for the estimation of over 50 airship aerodynamic model parameters. They augmented the system with 50 additional state variables which increased their computational burden. The proposed work is inspired by [29,36] and suggests an improved method that is based on an online estimation scheme utilizing the UKF algorithm for estimating the airship aerodynamic model in the form of forces and torques. It incorporates only six additional state variables, in which three are used for estimating the airship drag, side and lift forces, and the other three estimate roll, pitch and yaw moments. The method makes an assumption that the airship aerodynamic model is not available and also the rate of change of augmented states is zero because as compared to conventional drones, the airship has slow dynamics and the variation of aerodynamic forces acting on it is slow while it cruises through the air. For example, the rate of change of drag force acting on "UETT" airship and "YEZ-2A" airship is $\left|\dot{F}_{Ax}\right| \leqslant 3\times10^{-3}$ and $\left|\dot{F}_{Ax}\right| \leqslant 3\times10^{-2}$ respectively. The proposed UKF, online estimated, aerodynamic model information can be used to enhance the performance of model-based nonlinear controllers for airship automatic flight. Equation (15) states the proposed augmented state variables in which F_{Ax}, F_{Ay}, F_{Az} represent drag, side, and lifting aerodynamic forces and τ_{Al}, τ_{Am}, τ_{An} represent rolling, pitching, and yaw aerodynamic torques.

$$\boldsymbol{X}_{Ad} = [\ F_{Ax} \quad F_{Ay} \quad F_{Az} \quad \tau_{Al} \quad \tau_{Am} \quad \tau_{An}\ ]^{\mathrm{T}} \tag{15}$$

The rate of the aerodynamic force vector is given in

$$\dot{\boldsymbol{X}}_{Ad} = 0. \tag{16}$$

The above introduced variables are incorporated in the airship model given in (1) and the extended model that can be used for UKF implementation is given by

$$\begin{bmatrix} \dot{\boldsymbol{V}}_b \\ \dot{\boldsymbol{X}}_{Ad} \end{bmatrix} = \begin{bmatrix} \boldsymbol{M}^{-1}(\boldsymbol{F}_d + \boldsymbol{X}_{Ad} + \boldsymbol{F}_{As} + \boldsymbol{F}_P) \\ \boldsymbol{0}_{6\times1} \end{bmatrix}. \tag{17}$$

Let $\boldsymbol{f}_e = \boldsymbol{F}_d + \boldsymbol{X}_{Ad} + \boldsymbol{F}_{As} + \boldsymbol{F}_P$, $\boldsymbol{f}_e = [f_{eu} \quad f_{ev} \quad f_{ew} \quad \tau_{el} \quad \tau_{em} \quad \tau_{en}]^{\mathrm{T}}$, then the modified body axes force vector $\boldsymbol{f}_e$ can be written down as

$$f_{e1} = -m_z wq + m_y rv + m\left[a_x\left(q^2+r^2\right) - a_z rp\right] + F_{Ax} - (W-B)\sin\theta + (T_{ds}+T_{dp})\cos\mu, \tag{18}$$

$$f_{e2} = -m_x ur + m_z pw + m[-a_x pq - a_z rq] + F_{Ay} + (W - B\cos\theta\sin\phi), \tag{19}$$

$$f_{e3} = -m_y vp + m_x qu + m\left[-a_x rp + a_z\left(q^2+p^2\right)\right] + F_{Az} + (W-B)\cos\theta\cos\phi - (T_{ds}+T_{dp})\sin\mu, \tag{20}$$

$$f_{e4} = -(J_z - J_y)rq + J_{xz}pq + ma_z(ur - pw) + \tau_{Al} + a_z W\cos\theta\sin\phi + (T_{dp}-T_{ds})\sin\mu d_y + (T_{ds}+T_{dp})(d_z\cos\mu - d_x\sin\mu), \tag{21}$$

$$f_{e5} = -(J_x - J_z)pr + J_{xz}\left(r^2-p^2\right) + m[a_x(vp-qu) - a_z(wq - rv)] + \tau_{Am} - (a_z W - b_z B)\sin\theta - (a_x W - b_x B)\cos\theta\cos\phi, \tag{22}$$

$$f_{e6} = -(J_y - J_x)qp - J_{xz}qr + m[-a_x(ur-pw)] + \tau_{An} + a_x W\cos\theta\sin\phi + (T_{dp}-T_{ds})\cdot\cos\mu d_y. \tag{23}$$

The modified nonlinear state-space form, augmented with additional state variables, in the compact vector form is given in

$$\begin{bmatrix} \dot{\boldsymbol{\xi}} \\ \dot{\boldsymbol{\upsilon}} \\ \dot{\boldsymbol{X}}_{Ad} \end{bmatrix} = \begin{bmatrix} \boldsymbol{R}(\varsigma) & \boldsymbol{0}_{6\times6} \\ \boldsymbol{0}_{6\times6} & \boldsymbol{M}^{-1} \\ \boldsymbol{0}_{6\times6} & \boldsymbol{0}_{6\times6} \end{bmatrix} \begin{bmatrix} \boldsymbol{\upsilon} \\ \boldsymbol{f}_e \\ \boldsymbol{0}_{6\times1} \end{bmatrix}. \tag{24}$$

The new extended airship state vector is given by

$$\boldsymbol{X} = [\ \boldsymbol{\zeta} \quad \boldsymbol{\varsigma} \quad \boldsymbol{\nu} \quad \boldsymbol{\omega} \quad \boldsymbol{X}_{Ad}\ ]^{\mathrm{T}}. \tag{25}$$

For estimator design, availability of position and attitude estimates is considered, so the UKF algorithm utilizes the measurement vector given in (26) for the calculation of estimation error. The estimation error is used for the correction of estimated states.

$$\boldsymbol{Y} = \boldsymbol{C}\boldsymbol{X} = [\boldsymbol{I}_{6\times6} \ \ \boldsymbol{0}_{6\times12}]\boldsymbol{X} \tag{26}$$

where $\boldsymbol{C}$=$[\boldsymbol{I}_{6\times6} \quad \boldsymbol{0}_{6\times12}]$, $\boldsymbol{I}_{6\times6}$ is an identity matrix, $\boldsymbol{Y}$ is the measurement vector. Equation (24) represents the airship modified nonlinear model in the continuous time state-space form for estimator design. Its compact vector form is given by

$$\dot{\boldsymbol{X}} = f(\boldsymbol{X}, \boldsymbol{u}). \tag{27}$$

For the discrete-time implementation of the algorithm, first-order Euler integration is performed of the system (27). Further, it is extended with the incorporation of process and measurement noise. The resulted system is given by

$$\boldsymbol{X}_{k+1} = \boldsymbol{I}\boldsymbol{X}_k + \boldsymbol{T}_s f(\boldsymbol{X}_k, \boldsymbol{u}_k) + \boldsymbol{w}_p, \tag{28}$$

$$\boldsymbol{Y}_k = \boldsymbol{C}\boldsymbol{X}_k + \boldsymbol{w}_m, \tag{29}$$

where $\boldsymbol{I}$ is the identity matrix, $\boldsymbol{X}_k$ is the airship discrete-time state vector at sampling instant k, $\boldsymbol{T}_s$ represents the system sampling time, $\boldsymbol{u}_k$ represents the system input vector and in the airship case it consists of propeller input, rudder, and elevator deflections. The process and measurement noises are incorporated as $\boldsymbol{w}_p$ and $\boldsymbol{w}_m$ vectors respectively. They are Gaussian white noise vectors with zero mean.

The UKF algorithm consists of two main steps: prediction and correction. In the prediction step, the system model is used for the prediction of the system state vector for the next sampling time, and in the correction step, the predicted states are corrected using Kalman gain and estimation error. The process noise covariance matrix is represented by $\boldsymbol{Q}$ and the measurement noise covariance matrix is represented by $\boldsymbol{R}$. They are diagonal matrixes and they are used as the tuning parameters. In the airship state estimation case, many iterations are used to tune them. The airship state error covariance matrix is given by $\boldsymbol{P}_k$. The UKF algorithm at each sampling time is summarized as follows.

(i) Prediction

i) Choose the sigma points χ_k^j at time step k.

$$\widehat{\chi}_k^{(0)} = \widehat{\boldsymbol{X}}_k \tag{30}$$

$$\widehat{\chi}_k^j = \widehat{\boldsymbol{X}}_k + \Delta \boldsymbol{X}^{(j)},\ \ j = 1,\cdots,2N \tag{31}$$

$$\Delta \boldsymbol{X}^{(j)} = \left(\sqrt{N\boldsymbol{P}_k}\right)_j,\ \ j = 1,\cdots,N \tag{32}$$

$$\Delta \boldsymbol{X}^{(N+j)} = -\left(\sqrt{N\boldsymbol{P}_k}\right)_j,\ \ j = 1,\cdots,N \tag{33}$$

ii) Use the nonlinear system modelling equation for the calculation of predicted states for each sigma point.

$$\widehat{\boldsymbol{X}}_{k+1}^j = f(\widehat{\chi}_k^j, \boldsymbol{u}_k) \tag{34}$$

iii) Combine the predicted states to obtain the predicted states at time $k+1$.

$$\widehat{\boldsymbol{X}}_{k+1} = \sum_{j=0}^{2N} W_N^j \widehat{\boldsymbol{X}}_k^j \tag{35}$$

$$W_N^j = \frac{1}{2N},\ \ j = 1,2,\cdots,2N \tag{36}$$

iv) Compute the covariance of the predicted state. Add $\boldsymbol{Q}_k$ to account for the additive process noise.

$$\boldsymbol{P}_{k+1} = \sum_{j=0}^{2N} W_c^j \left(\widehat{\chi}_{k-1}^{(j)} - \widehat{\boldsymbol{X}}_k\right)^{\mathrm{T}} \left(\widehat{\chi}_k^{(j)} - \widehat{\boldsymbol{X}}_k\right)^{\mathrm{T}} + \boldsymbol{Q}_k \tag{37}$$

$$W_c^j = \frac{1}{2N},\ j = 1,2,\cdots,2N \tag{38}$$

(ii) Correction

i) Select sigma points for N number of states and have k as sampling instant.

$$\widehat{\chi}_k^{(0)} = \widehat{\boldsymbol{X}}_{k-1} \tag{39}$$

$$\widehat{\chi}_k^j = \widehat{\boldsymbol{X}}_{k-1} + \Delta \boldsymbol{X}^{(j)},\ \ j = 1,\cdots,2N \tag{40}$$

$$\Delta \boldsymbol{X}^{(j)} = \left(\sqrt{N\boldsymbol{P}_{k-1}}\right)_j,\ \ j = 1,\cdots,N \tag{41}$$

$$\Delta \boldsymbol{X}^{(N+j)} = -\left(\sqrt{N\boldsymbol{P}_{k-1}}\right)_j,\ \ j = 1,\cdots,N \tag{42}$$

ii) Use the nonlinear measurement function for the calculation of predicted measurements.

$$\widehat{\boldsymbol{Y}}_k^j = h(\widehat{\chi}_{k-1}^{(j)}, \boldsymbol{u}_k),\ \ i = 0,1,\cdots,2N \tag{43}$$

iii) In this step, predicted measurements at previous time instants are combined and predicted measurements for time instant k are obtained.

$$\widehat{\boldsymbol{Y}}_k = \sum_{j=0}^{2N} W_N^j \widehat{\boldsymbol{Y}}_{k-1}^j \tag{44}$$

iv) Estimate the covariance of predicted measurements, where $\boldsymbol{R}_k$ accounts for additive measurement noise.

$$\boldsymbol{P}_y = \sum_{j=0}^{2N} W_c^j \left(\widehat{\boldsymbol{Y}}_{k-1}^{(j)} - \widehat{\boldsymbol{Y}}_k\right)^{\mathrm{T}} \left(\widehat{\boldsymbol{Y}}_{k-1}^{(j)} - \widehat{\boldsymbol{Y}}_k\right)^{\mathrm{T}} + \boldsymbol{R}_k \tag{45}$$

v) Estimate the cross-covariance between $\widehat{\boldsymbol{X}}_k$ and $\widehat{\boldsymbol{Y}}_k$.

$$\boldsymbol{P}_{xy} = \frac{1}{2N} \sum_{j=0}^{2N} \left(\widehat{\chi}_{k-1}^{(j)} - \widehat{\boldsymbol{X}}_{k-1}\right) \left(\widehat{\boldsymbol{Y}}_{k-1}^{(j)} - \widehat{\boldsymbol{Y}}_k\right)^{\mathrm{T}} \tag{46}$$

The summation starts from $j = 1$ because $\widehat{\boldsymbol{X}}_{k-1}^0 - \widehat{\boldsymbol{X}}_{k-1} = 0$.

vi) Obtain the estimated state and the state estimation error covariance at time step k.

$$\boldsymbol{K}_k = \boldsymbol{P}_{xy} \boldsymbol{P}_y^{-1}, \tag{47}$$

$$\widehat{\boldsymbol{X}}_k = \widehat{\boldsymbol{X}}_{k-1} + \boldsymbol{K}_k (\boldsymbol{Y}_k - \widehat{\boldsymbol{Y}}_k), \tag{48}$$

$$\boldsymbol{P}_k = \boldsymbol{P}_{k-1} - \boldsymbol{K}_k \boldsymbol{P}_y \boldsymbol{K}_k^{\mathrm{T}}, \tag{49}$$

where $\boldsymbol{K}_k$ is the Kalman gain at sampling instant k.

In (41) and (42), $\boldsymbol{P}_{k-1} \in \mathbf{R}^{18\times 18}$ represents the state estimation error covariance matrix at the previous time step. It is a symmetric positive definite matrix. Its initial value is carefully selected because a large value can cause overshoot in the transient response and it may diverge the filter and a small value slows down the filter convergence.

In the current case, many iterations are performed to tune it. In the correction and prediction steps, it is updated by using Kalman filter gain and state covariance, and using a previous value of the state estimation error covariance matrix as given in (37) and (49) of correction and prediction steps respectively. $\boldsymbol{Q} \in \mathbf{R}^{18\times18}$ in (37) represents the process noise covariance matrix. It is treated as a tuning parameter for the filter. It has 18 diagonal entries in which the first 12 which represent the position, attitude, linear and angular velocities have modelling equation available and the last six which represent aerodynamic forces and torques have no modelling equations. Therefore, magnitudes of its first 12 diagonal entries are kept small and the last six entries are tuned accordingly. $\boldsymbol{K} \in \mathbf{R}^{18\times1}$ in (47) is Kalman gain. Cross-covariance of predicted states is used to calculate it. Kalman gain corrects the predicted states according to the measurement error.

4. Simulation results

For the evaluation of UKF performance, a simulation environment is developed for the "UETT" experimental airship based on Matlab/Simulink. The "UETT" airship project was started in 2013 at the University of Engineering and Technology, Taxila, Pakistan. The project aims to develop an autonomous navigation control system for airships so that the airship can be utilized for monitoring tasks. Equations (1)−(14) are implemented with the parameters provided in Table 1. The "UETT" airship is fed with propeller input, elevator, and rudder deflections in specific time intervals. Initially, it is assumed that the airship is hovering at 100 m altitude under the neutral buoyancy condition. Further, it is assumed that weather and temperature remain constant.

After 3 s, the thruster input is applied to the airship and it starts moving with forward velocity as shown in Fig. 2 (a). Thruster force changes airship hover condition and initially it executes oscillatory motion about y-axes that can be observed from Fig. 2 (d) and Fig. 2 (e) where changes can be observed in pitch rate and vertical velocity. The oscillatory motion exists because unlike conventional airplanes, an airship is lighter than air as compared to its large volume, and also its thrusters are mounted on the front side of the gondola slightly forward to CV and CG points. However, the oscillations decay out after 30 s of flight when the airship achieves its steady-state forward velocity. In steady-state, without the application of rudders and elevators inputs, the airship moves forward in body axes x-direction having slightly nose up configuration. During this motion, the airship experiences aerodynamic "drag force" as shown in Fig. 3 (a). From the plots, it can be observed that as the airship velocity increases, the drag force also increases and when an airship achieves its steady-state velocity, then the drag force takes a constant value of −4 N.

Table 1 Parameters of the airship under consideration

Parameter	Symbol	Value
Length	L/m	9
Diameter	D/m	2.2
Volume of hull	V/m^3	25
Mass	m/kg	24.073
Moment of inertia about x-axis	I_x/kg·m^2	2.842
Moment of inertia about y-axis	I_y/kg·m^2	26.769
Moment of inertia about z-axis	I_z/kg·m^2	26.769
Product of inertia	I_{xz}/kg·m^2	0.001 166
Maximum radius	b/m	1.1
x-distance from nose to CV	a_1/m	3.9
x-distance from CV to tail	a_2/m	5.1
Distance of CV from airship nose on x-axis	x_{cv}/m	4.34
Length of the hull up to the leading edge of the fins	l_h/m	6.43
x-distance from origin to aerodynamic center of fins	l_{f1}/m	2.41
z-distance from origin to aerodynamic center of fins	l_{f3}/m	1.04
x-distance from origin to geometric center of fins	l_{f2}/m	2.62
Fin reference area	S_f/m^2	9
Gondola reference area	S_g/m^2	1

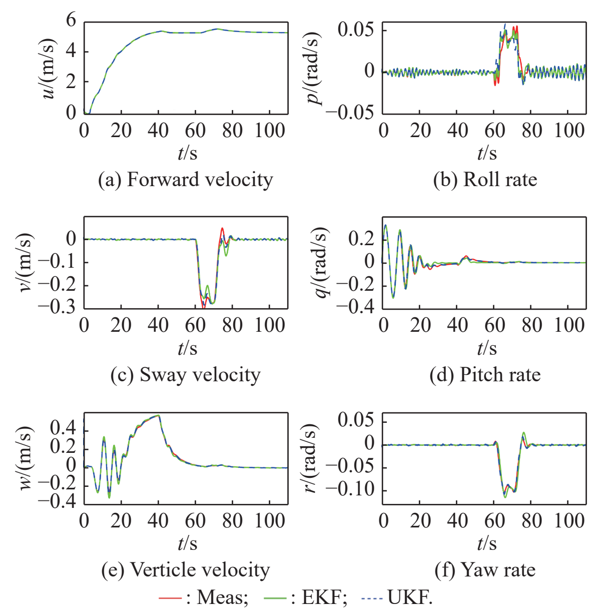

Fig. 2 Airship states estimation

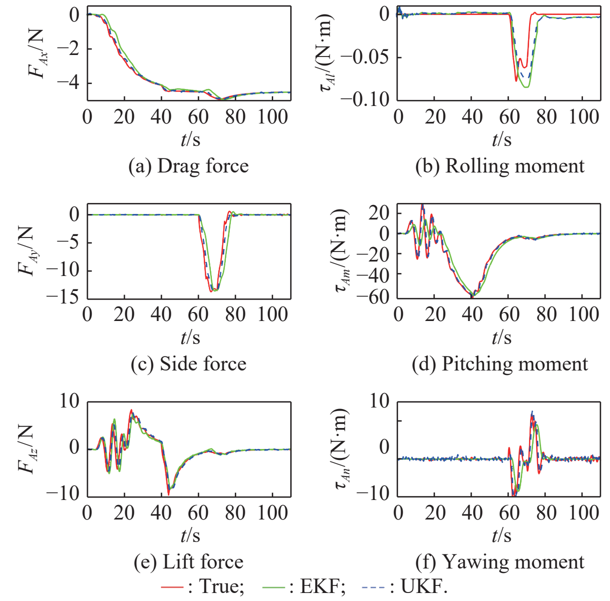

(a) Drag force (b) Rolling moment (c) Side force (d) Pitching moment (e) Lift force (f) Yawing moment

Fig. 3 Airship aerodynamic forces and aerodynamic torques estimation

Before the pitch rate settles down to zero, the elevator input is applied after 20 s of flight. Elevator deflection introduces longitudinal motion. Airship longitudinal motion can be observed by changes that occur in vertical velocity and pitch rate as shown in Fig. 2 (e) and Fig. 2 (d). From Fig. 2 (e) it can be seen that the elevator input changes the vertical velocity from its initial value to 0.4 m/s and after 40 s when the input is removed, it slowly goes down to zero. The vertical motion of the airship is actually a consequence of lifting aerodynamic force and aerodynamic pitching moment as shown in Fig. 3 (e) and Fig. 3 (d). From the plots, it can be observed that the elevator input produces aerodynamic lift force and pitching moment. They gain the value of −10 N and −60 N·m respectively; however, the removal of input causes their values to become zero.

After 60 s of flight, the rudder input is applied and it changes sway velocity, roll rate, and yaw rate as shown in Fig. 2. Fig. 2 (c) shows that the application of rudder deflection causes sway velocity to gain −0.3 m/s of velocity and becomes zero after the removal of input. From Fig. 2 (f) change of yaw rate can be observed and the input also causes roll rate to change its value as shown in Fig. 2 (b). This is because air vehicles tilt with some angle while turning due to rolling aerodynamic torques that act because of rudder deflection. And on the removal of rudder deflection the airship again takes its initial attitude. The aerodynamic side force and yaw moment can be seen in Fig. 3 (c) and Fig. 3 (f) that acts on the airship during its turning. Airship tilt is due to the rolling aerodynamic moment as shown in Fig. 3 (b).

Airship states and aerodynamic forces and torques plots given in Fig. 2 and Fig. 3 also show the UKF estimations. Airship body axes linear and angular velocities can be seen in Fig. 2. UKF estimated airship aerodynamic forces and aerodynamic torques are shown in Fig. 3. From the plots, one can conclude that the estimation performance of UKF for airship actual states and for auxiliary states is good. But how much good that performance is? It is quantified by doing some sort of error analysis. In order to get the confidence on estimator performance, estimation error, error covariance, and mean error are calculated. Also, the 2-σ uncertainty bounds (UBs) of error variance are calculated for UKF estimated states. The estimation error should be of small magnitude, it should have zero mean and it should be uncorrelated except at zero lag. Additionally, for 2-σ UBs, the statistical 68–95–99.7 rule says that 95% of the data should lie within two standard deviations about the mean value. The mean error is calculated by using the formula given as

$$M_e = \frac{1}{N}\sum_{i=0}^{i=t}(\text{True value}(i) - \text{Estimated value}(i)) \qquad (50)$$

where M_e is the mean estimation error value. M_e for all estimated states are calculated and given in Table 2. From the table data, it can be observed that the estimation error follows the specified judgment criteria.

Table 2 Mean estimation error of EKF and UKF for state estimation

State	Mean estimation error	
	EKF	UKF
u	0.013 6	0.012 8
v	$-2.278\,0\times10^{-5}$	$-2.521\,0\times10^{-5}$
w	0.001 7	0.001 4
P	0.003 6	0.003 5
q	0.004 5	0.004 1
r	$6.707\,0\times10^{-5}$	$6.208\,0\times10^{-5}$
F_{Ax}	−0.112 3	−0.034
F_{Ay}	0.009 2	−0.004 0
F_{Az}	−0.005 5	0.002 2
τ_{Al}	−0.002 0	0.001 2
τ_{Am}	−0.250 1	−0.064 5
τ_{An}	0.013 0	0.015 3

The following formula is used for finding the percentage of data exceeding the uncertainty bounds:

$$\boldsymbol{D}_{FB} = \left|\boldsymbol{e}_i - \sqrt{\boldsymbol{P}_i}\right|, \qquad (51)$$

$$\text{Exceed} = \frac{\text{number of nonzero elements in } \boldsymbol{D}_{FB}}{\text{total number of elements in } \boldsymbol{e}_i \text{ vector}} \times 100\%, \tag{52}$$

where $\boldsymbol{D}_{FB}$ is the vector containing the distance of error exceeding the UBs, $\boldsymbol{e}_i$ is the vector containing the estimation error of the ith state and $\boldsymbol{P}_i$ is the vector comprising of error covariance of the ith state at each sampling instant. For the present case, the above-mentioned error analysis is performed for each state as shown in Fig. 4 and Fig. 5.

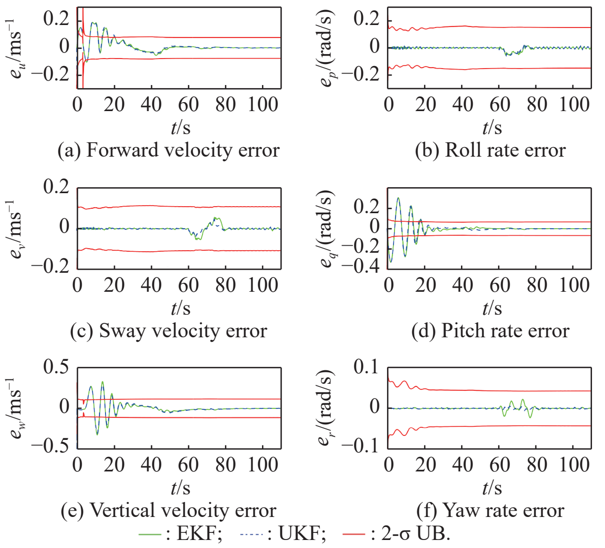

Fig. 4 Estimation error and 2-σ UB plots for linear and angular velocities

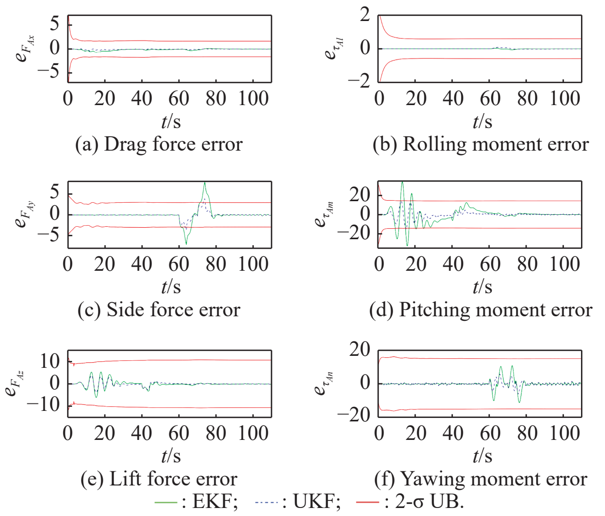

Fig. 5 Estimation error and 2-σ UB plots for aerodynamic forces and torques estimation

Using (51) and (52), percentages of errors exceeding the prescribed bounds are calculated and in the case of UKF's estimation, Fig. 4 shows that for estimating the forward velocity, vertical velocity, and pitch rate, about 3%, 5%, and 4% of the error are exceeding the specified bounds but for other states, 100% of error stays within the UBs. In Fig. 5, for estimating side force, lift force, pitching moment, and yaw moment, 1.64%, 3.28%, 4.97%, and 5% of estimation error are exceeding the bounds. These observations show that for actual and augmentative states, the UKF estimator fulfills the minimum error criteria.

For comparative study, EKF is also implemented for the same problem and its results are compared with UKF. From the results, it can be seen that for linear and angular velocities estimation, both filter's performances are the same but for aerodynamic forces and aerodynamic torques, estimation error for EKF is more than that for UKF which can be seen from Table 2. It shows that UKF performs better than EKF. From 2-σ UBs perspective, for estimating side force, lift force, pitching moment, and yawing moment using EKF, about 9.8%, 8.4%, 5.4%, and 8.5% respectively, of the estimation error are exceeding the prescribed bounds and it slightly violates the minimum error criteria. From this analysis, we can conclude that for the present case, UKF performs superior to EKF.

In order to check the computational overhead of both algorithms, few test scenarios are used in which running times for each algorithm is recorded. The simulation is performed on core i5 having 2.3 GHz speed on Matlab 2019a software. According to the observations, on average the EKF algorithm takes 130.78 m per estimate and the UKF algorithm takes 586.27 m per estimate. The computational intensiveness of the UKF algorithm is obvious because it has to handle all sigma points and it performs 15 Runge-Kutta integrations to propagate the sigma points. If Julier and Uhlmann's method is used for reducing the number of sigma points [37], it will require eight Runge-Kutta integrations, however, the EKF algorithm needs only one integration to complete the computation. In the airship case, 12 are the actual state variables and six are the augmented ones, so a total of 18 states require the computation of a large Jacobian matrix [38]. If the numerical computation method for calculating the Jacobean matrix is used, then EKF will require more computational time. Also, the analytical calculation of the Jacobian matrix is cumbersome but reduces the computational overhead. However, in the case of UKF, the computation of the Jacobian matrix is not required.

From the above discussion, we can conclude that for airship states, aerodynamic forces, and aerodynamic torques estimation, UKF algorithm performance is better than EKF but with the cost of computational overburden. As the airship is a slow-moving platform and has slow dynamics owing to its large size, in our case we can prefer UKF over EKF estimation as the former provides more accuracy.

5. Conclusions

In this paper, airship body axes state that consists of its linear velocities (u,v,w), angular velocities (p,q,r), aerodynamic forces (F_{Ax},F_{Ay},F_{Az}), and aerodynamic torques $(\tau_{Al},\tau_{Am},\tau_{An})$ are successfully estimated using UKF. The estimator assumes that airship position and attitude estimations are available. Estimator performance is validated in a nonlinear open-loop simulation environment developed for "UETT" airship, where the airship is provided with thruster, rudder, and elevator inputs. For estimator design, the airship nonlinear 6-DOF model is modified and six auxiliary state variables are introduced. In the modified model, it is assumed that expressions for the aerodynamic model are not available and newly introduced state variables capture their effect. Based on this new formulation, UKF is designed. In order to get the confidence on estimates, estimation error and 2-σ uncertainty bounds are calculated which shows that the estimator performs reasonably well. EKF is also implemented under the same scenario and its results are compared with UKF. The comparison shows that UKF slightly outperforms the EKF. These estimates can be utilized for the development of the nonlinear autonomous flight controller for an airship. Although the robust controller deals with model uncertainties, however, their performance can be increased if that information is provided to them online. In the future work, a nonlinear flight controller will be designed for airship autonomous navigation and the controller will be provided with UKF estimated states and model information.

References

[1] STOCKBRIDGE C, CERUTI A, MARZOCCA P. Airship research and development in the areas of design, structures, dynamics and energy systems. International Journal of Aeronautical & Space Sciences, 2012, 13(2): 170–187.

[2] BUENO S S, AZINHEIRAETAL J R, RAMOS J, et al. Project AURORA: towards an autonomous robotic airship. Proc. of the IEEE International Conference on Intelligent Robots and Systems, 2002: 43−54.

[3] CHEN L, ZHANG H, DUAN D P. Control system design of a multi vectored thrust stratospheric airship. Proc. of the Institution of Mechanical Engineers, 2014, 228(11): 2045–2054.

[4] MILLER S H, FESEN R, HILLENBRAND L A, et al. Airships: a new horizon for science. https://arxiv.org/ftp/arxiv/papers/1402/1402.6706.pdf.

[5] COOK M V. The linearized small perturbation equations of motion for an airship. https://dspace.lib.cranfield.ac.uk/bitstream/handle/1826/1482/CIT_MISC_47.pdf;jsessionid=4C880D00DFB67F00383778B678C1CD31?sequence=3.

[6] KHOURY G A. Airship technology. Cambridge: Cambridge University Press, 2012.

[7] KORNIENKO A. System identification approach for determining flight dynamical characteristics of an airship from flight data. Stuttgart: University of Stuttgart, 2006.

[8] AHSAN M, CHOUDHRY M A. System identification of an airship using trust region reflective least squares algorithm. International Journal of Control, Automation and Systems, 2017, 15(3): 1384–1393.

[9] MAZHAR F, CHOUDHRY M A, SHEHRYAR M. Nonlinear auto-regressive neural network for mathematical modelling of an airship using experimental data. Proc. of the Institution of Mechanical Engineers, 2019, 233(7): 2549–2569.

[10] ZHANG J S, YANG X X, DENG X L, et al. Trajectory control method of stratospheric airships based on model predictive control in wind field. Proc. of the Institution of Mechanical Engineers, Part G: Journal of Aerospace Engineering, 2019, 233(2): 418–425.

[11] YANG Y N, WU J, ZHENG W. Positioning control for an autonomous airship. Journal of Aircraft, 2016, 53(6): 1638–1646.

[12] YANG Y N, WU J, ZHENG W. Adaptive fuzzy sliding mode control for robotic airship with model uncertainty and external disturbance. Journal of Systems Engineering and Electronics, 2012, 23(2): 250–255.

[13] MIAO J G, ZHOU J H, NIE Y, et al. Yaw controller design of stratospheric airship based on phase plane method. Chinese Journal of Aeronautics, 2016, 29(3): 738–745.

[14] XIAO C, HAN D, WANG Y Y, et al. Fault-tolerant tracking control for a multi-vectored thrust ellipsoidal airship using adaptive integral sliding mode approach. Proceedings of the Institution of Mechanical Engineers, Part G: Journal of Aerospace Engineering, 2018, 232(10): 1911–1924.

[15] XIAO C, WANG Y Y, ZHOU P F, et al. Adaptive sliding mode stabilization and positioning control for a multi-vectored thrust airship with input saturation considered. Transactions of the Institute of Measurement and Control, 2018, 40(15): 4208–4219.

[16] FOSSEN T I. Guidance and control of ocean vehicles. New York: Wiley, 1998: 5−56.

[17] JONES R. The aerodynamical characteristics of the airship as deduced from experiments on models, with application to motion in a horizontal plane. Journal of Royal Aeronautical Society, 1924, 28(158): 88–150.

[18] CURTISS H C, HAZEN D C, PUTMAN W F. LTA aerodynamic data revisited. Journal of Aircraft, 1976, 13(11): 835–844.

[19] GOMES S B V. An investigation into the flight dynamics of airships with application to the YEZ-2A. Cranfield: Cranfield Institute of Technology, 1990.

[20] FUNK P, LUTZ T, WAGNER S. Experimental investigations on hull-fin interferences of the LOTTE airship. Aerospace Science and Technology, 2003, 7(8): 603–610.

[21] JONES S P, DELAURIER J D. Aerodynamic estimation techniques for aerostats and airships. Journal of Aircraft, 1983, 20(2): 120–126.

[22] MUNK M M. The aerodynamic forces on airship hulls. https://digital.library.unt.edu/ark:/67531/metadc53403/m1/1/.

[23] ALLEN H J, PERKINS E W. Characteristics of flow over inclined bodies of revolution. https://digital.library.unt.edu/ark:/67531/metadc58746/m1/4/.

[24] LI Y W, NAHON M. Modeling and simulation of airship dynamics. Journal of Guidance Control & Dynamics, 2007,

30(6): 1691–1700.
[25] MUELLER J B, PALUSZEKT M A, ZHAO Y Y. Development of an aerodynamic model and control law design for a high altitude airship. Proc. of the AIAA 3rd Unmanned Unlimited Technical Conference, Workshop and Exhibit, 2004: 1−17.
[26] ASHRAF M Z, CHOUDHRY M A. Dynamic modeling of the airship with Matlab using geometrical aerodynamic parameters. Aerospace Science & Technology, 2013, 25(1): 56–64.
[27] LIU S Q, SANG Y J, JIN H B. Robust model predictive control for stratospheric airships using LPV design. Control Engineering Practice, 2018, 81: 231–243.
[28] YANG Y N, WANG W Q, YAN Y. Adaptive backstepping neural network control for three dimensions trajectory tracking of robotic airships. CEAS Aeronautical Journal, 2017, 8(4): 579–587.
[29] SOLAQUE L, LACROIX S. Airship control. Multiple heterogeneous unmanned aerial vehicles. Berlin: Springer, 2007: 147−188.
[30] YANG Y. Nonlinear control and state estimation of holonomic indoor airship. Montreal: McGill University, 2012.
[31] MULLER J, PAUL O, BURGARD W. Probabilistic velocity estimation for autonomous miniature airships using thermal air flow sensors. Proc. of the IEEE International Conference on Robotics & Automation, 2012: 39−44.
[32] Navigation toolbox™: user's guide (R2019b). www.mathworks.com/help/pdf_doc/nav/nav_ug.pdf.
[33] Sensor fusion and tracking toolbox™: user's guide (R2019b). www.mathworks.com/help/pdf_doc/fusion/fusion_ug.pdf.
[34] WASIM M, ALI A. Estimation of airship aerodynamic forces and torques using extended Kalman filter. IEEE Access, 2020, 8: 70204−70215.
[35] HAUGEN F. State estimation with Kalman filter. http://techteach.no/fag/seky3322/0708/kalmanfilter/kalmanfilter.pdf.
[36] BUTT S S, ASCHEMANN H. Multi-variable integral sliding mode control of a two degrees of freedom helicopter. IFAC-Papers On Line, 2015, 48(1): 802–807.
[37] JULIER S J, UHLMANNJ K. Reduced sigma point filters for the propagation of means and covariances through nonlinear transformations. Proc. of the American Control Conference, 2002: 887−892.
[38] LAVIOLA J J. A comparison of unscented and extended Kalman filtering for estimating quaternion motion. Proc. of the American Control Conference, 2003: 2435−2440.

Biographies

WASIM Muhammad was born in 1990. He received his M.S. degree in electrical engineering from Electrical and Mechanical Engineering College, National University of Science and Technology, Islamabad, Pakistan. Currently, he is a Ph.D. student at the University of Engineering and Technology, Taxila, Pakistan. His research interest is control systems.
E-mail:muhammad077wasim@gmail.com

ALI Ahsan was born in 1977. He received his Ph.D. degree in control systems from Hamburg University of Technology, Germany. Currently, he is working as an assistant professor with the Department of Electrical Engineering at the University of Engineering and Technology, Taxila, Pakistan. His research interests include machine learning, model identification, linear parameter varying modeling, and control design.
E-mail: ahsan.ali@uettaxila.edu.pk